Electronic Supplementary Material (ESI) for Faraday Discussions


# Steric Effects for Proton, Hydrogen-Atom, and Hydride Transfer Reactions with Geometric Isomers of NADH-Model Ruthenium Complexes

*Brian W. Cohen,*[†] *Dmitry E. Polyansky,*[*,†] *Patrick Achord,*[†] *Diane Cabelli,*[†] *James T. Muckerman,*[†] *Koji Tanaka,*[§] *Randolph P. Thummel,*[‡] *Ruifa Zong,*[‡] *and Etsuko Fujita*[*,†]

[†] Chemistry Department, Brookhaven National Laboratory, Upton, New York 11973-5000, USA

[§] Institute for Molecular Science, 5-1 Higashiyama, Myodaiji, Okazaki, Aichi 444-8787, Japan

[‡] Department of Chemistry, University of Houston, Houston TX 77204-5003, USA

## Supporting Information

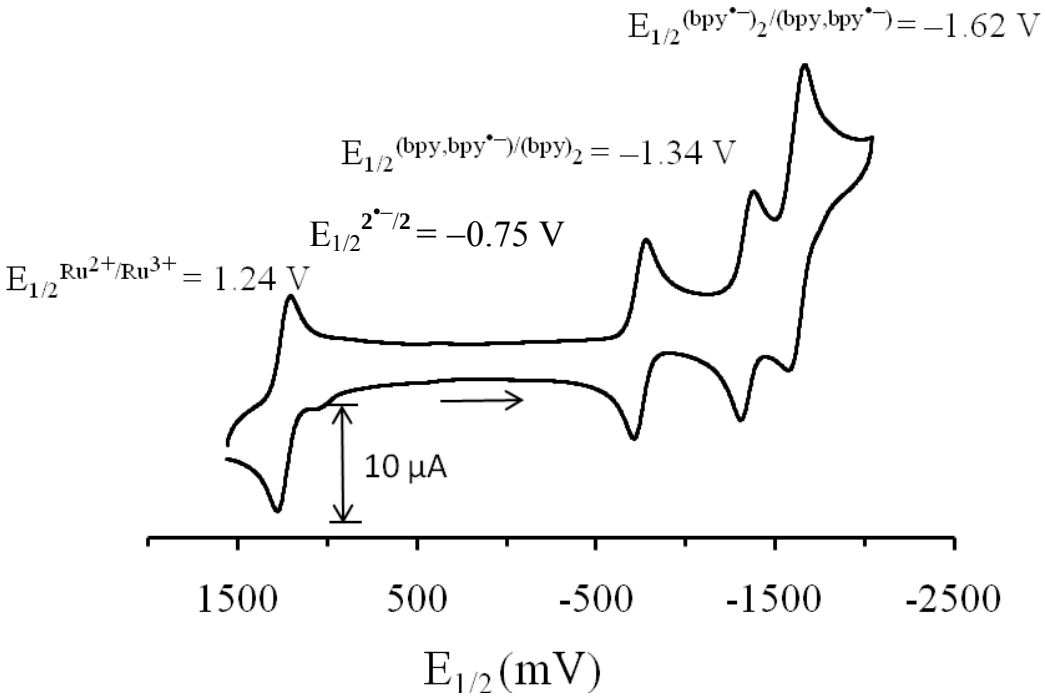


Figure S1. Cyclic voltammogram of [**Ru**(**2**)]$^{2+}$ in $CH_3CN$ versus SCE.

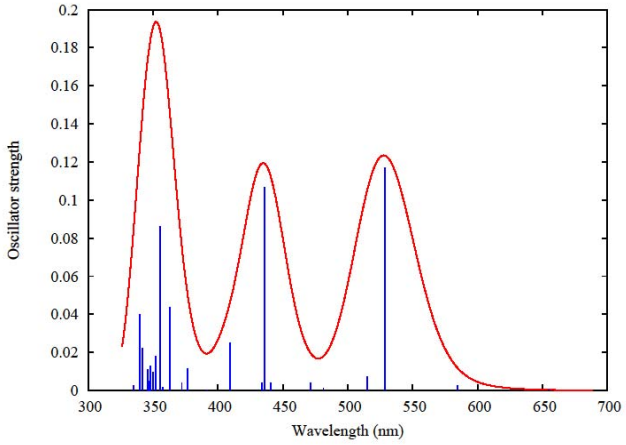


Assignments of the absorption bands of $[\mathbf{Ru(2)}]^{2+}$

| Peak | Percent | Transition | |
|---|---|---|---|
| 528 nm (2.3 eV) | 0.2 | HOMO-2 → LUMO | MLCT |
| | 0.21 | HOMO-1 → LUMO | MLCT |
| 436 nm (2.8 eV) | 0.35 | HOMO-2 → LUMO+1 | MLCT |
| | 0.08 | HOMO-1 → LUMO+2 | MLCT |
| 355 nm (3.5 eV) | 0.08 | HOMO-4 → LUMO | π→π* |
| | 0.12 | HOMO-2 → LUMO+3 | MLCT |
| | 0.15 | HOMO-1 → LUMO+4 | MLCT |

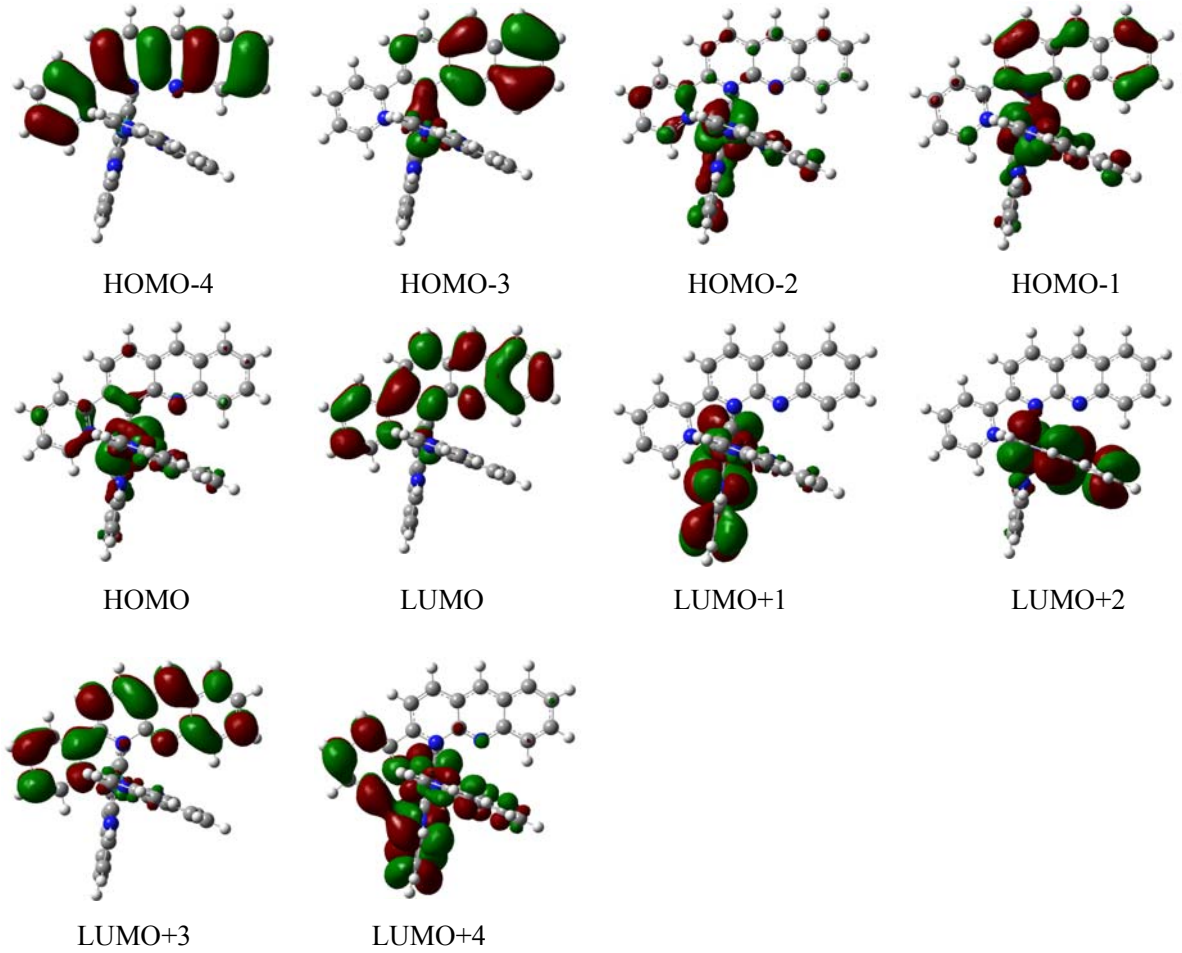


Figure S2. Calculated spectrum, assignment of absorption bands and the frontier orbitals of $[\mathbf{Ru(2)}]^{2+}$.

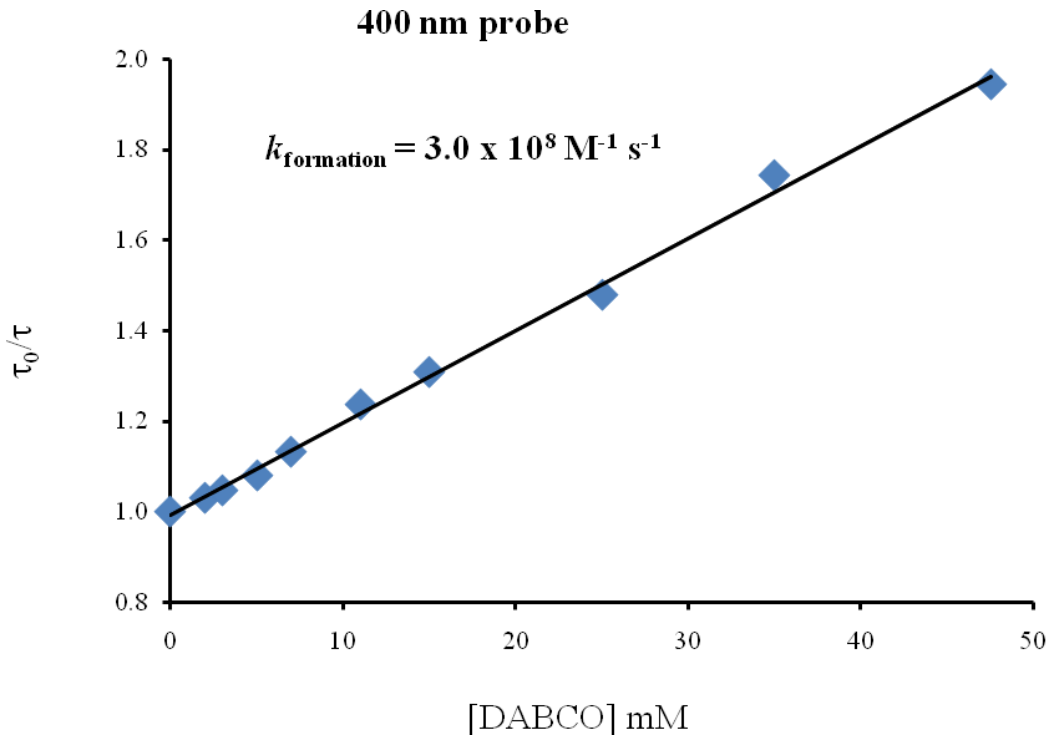


Figure S3. The bimolecular rate constant of quenching the excited state of [**Ru**(**2**)]$^{2+}$ by DABCO in acetonitrile.

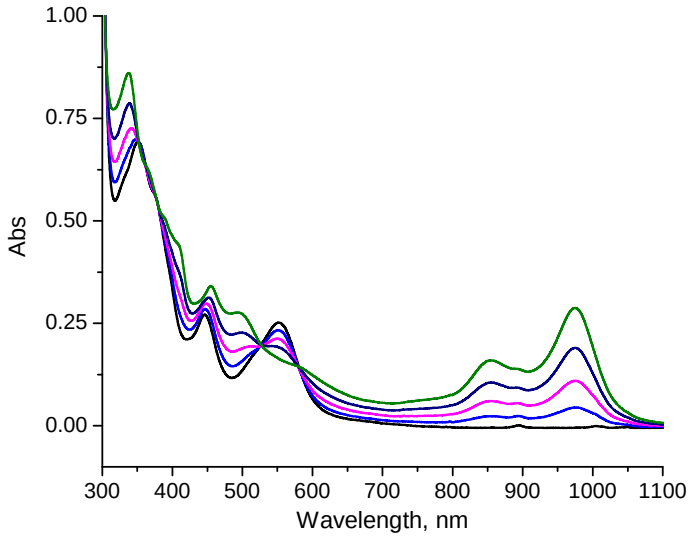


Figure S4. UV-vis-NIR absorption spectra of stepwise reduction of $[\mathbf{Ru}(\mathbf{2})]^{2+}$ (black) to $[\mathbf{Ru}(\mathbf{2}^{\bullet-})]^{+}$ (green) by Na/Hg amalgam in $CH_3CN$.

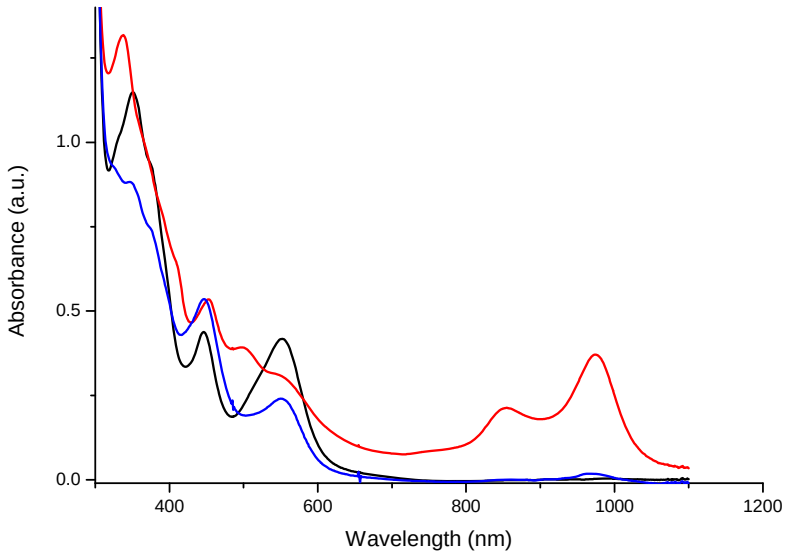


Figure S5. UV-vis-NIR spectra of photochemical formation of $[\mathbf{Ru}(\mathbf{2}^{\bullet-})]^{+}$ (red) from $[\mathbf{Ru}(\mathbf{2})]^{2+}$ (black) in $CH_3CN/NEt_3$. The blue spectrum measured after an addition of 10 eq. of $HClO_4$ to the $[\mathbf{Ru}(\mathbf{2}^{\bullet-})]^{+}$ solution indicates formation of a 1:1 mixture of $[\mathbf{Ru}(\mathbf{2})]^{2+}$ and $[\mathbf{Ru}(\mathbf{2}HH)]^{2+}$.

| | |
|---|---|
| 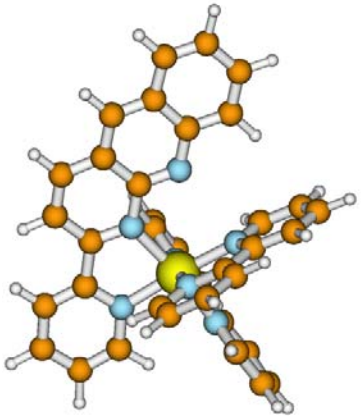 | 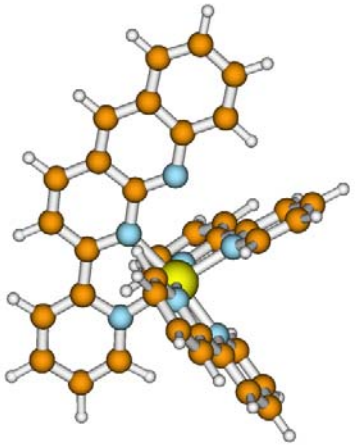 |
| $[\mathbf{Ru}(\mathbf{2})]^{2+}$ | $[\mathbf{Ru}(\mathbf{2}^{\bullet-})]^{+}$ |
| 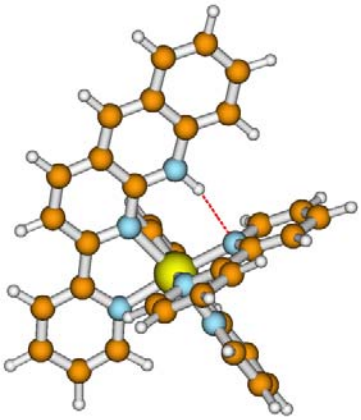 | 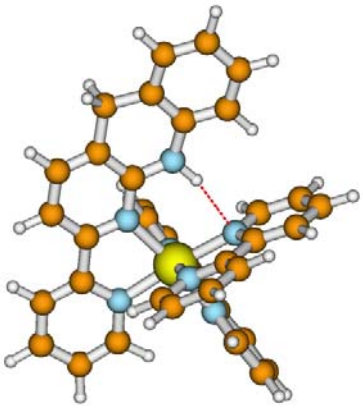 |
| $[\mathbf{Ru}(\mathbf{2H}^{\bullet})]^{2+}$ | $[\mathbf{Ru}(\mathbf{2}\mathrm{HH})]^{2+}$ |
| 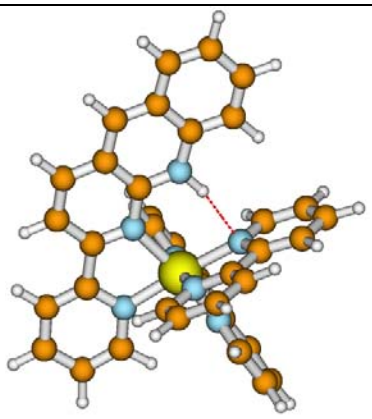 | 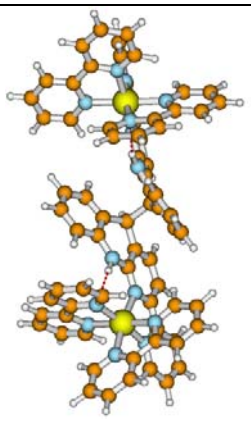 |
| $[\mathbf{Ru}(\mathbf{2}\mathrm{H})]^{3+}$ | Possible conformer of $[\mathbf{Ru}(\mathbf{2}\mathrm{H})]_2^{4+}$ |

Figure S6. Calculated structures of [**Ru**(**2**)]$^{2+}$, [**Ru**(**2**$^{\bullet-}$)]$^{+}$, [**Ru**(**2**H$^{\bullet}$)]$^{2+}$, [**Ru**(**2**HH)]$^{2+}$, [**Ru**(**2**H)]$^{3+}$ and a possible isomer of [**Ru**(**2**H)]$_2^{4+}$. The red line indicates an internal hydrogen bond between the protonated N atom and a coordinated N of the bpy ligand.

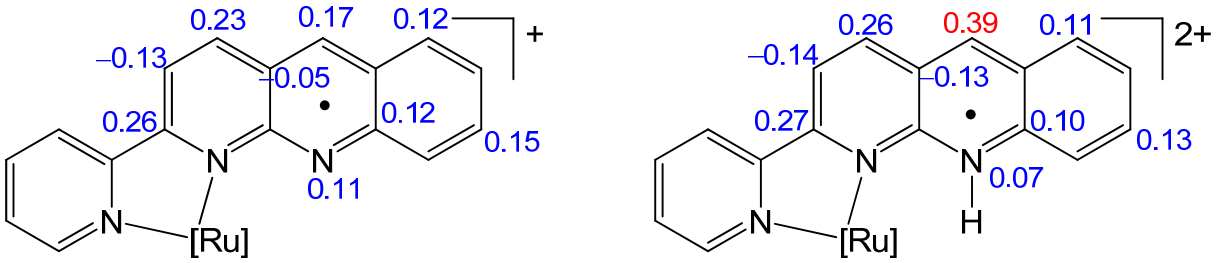


Figure S7. Calculated Mulliken atomic spin densities in [**Ru**(**2**$^{\bullet-}$)]$^{+}$ and protonated [**Ru**(**2H**$^{\bullet}$)]$^{2+}$.

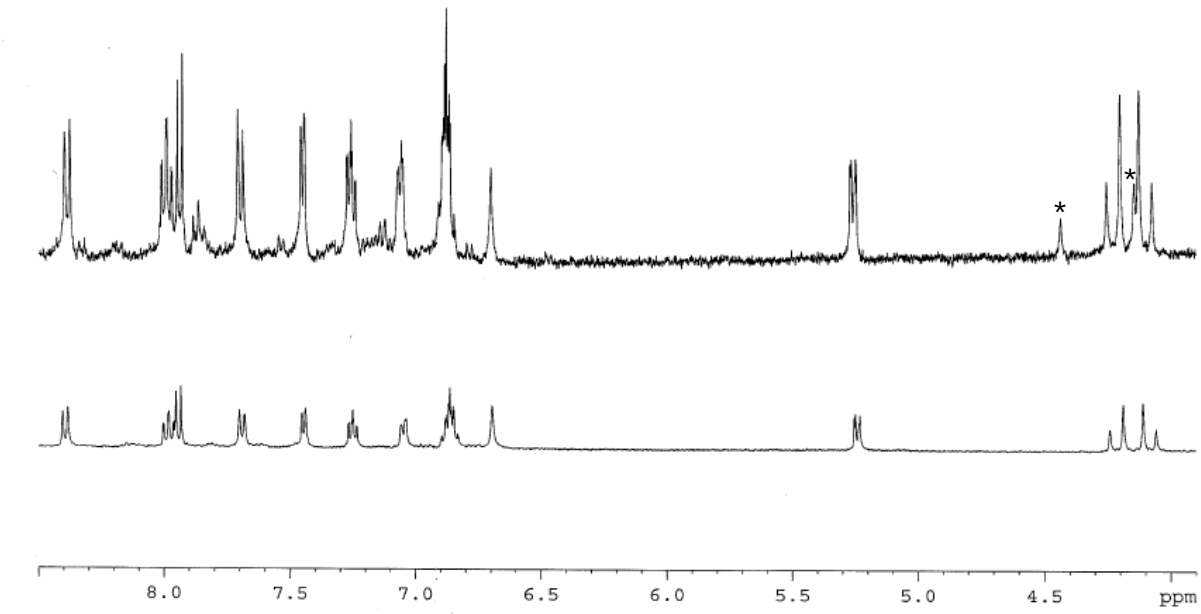


Figure S8. $^{1}$H NMR spectra of [**Ru**(**2**HH)]$^{2+}$ photochemically (top) and chemically (bottom) produced in $CD_3CN$. Impurities due to photodecomposition are labeled (*).

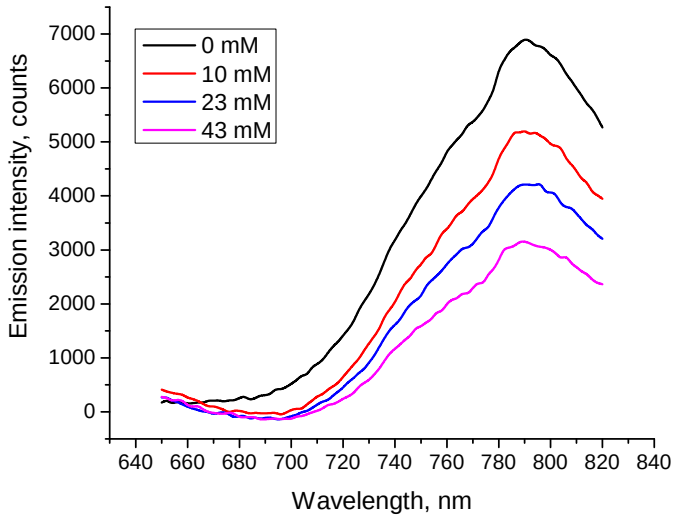


Figure S9. Uncorrected emission spectra of $[\mathbf{Ru}(\mathbf{1})]^{2+}$ in $CH_3CN$ (excitation at 528 nm) in the presence of different concentrations of $H_2Q$.

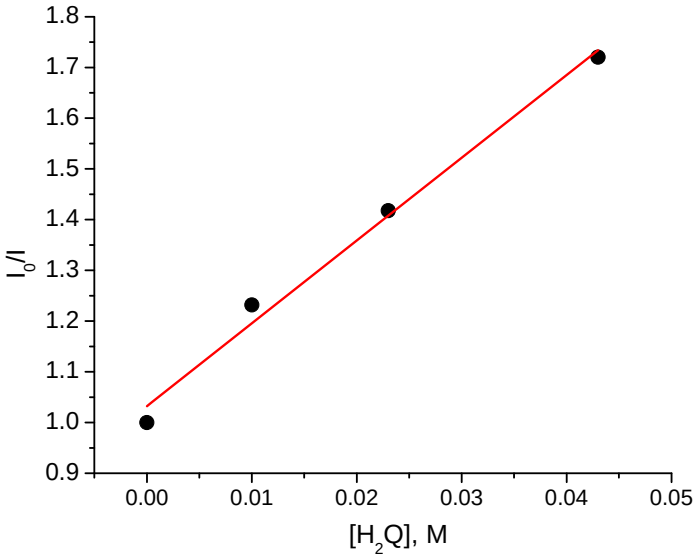


Figure S10. The plot of $I_0/I$ vs. concentration of $H_2Q$, where $I_0$ is the emission intensity in the absence of $H_2Q$. The red line is the linear fit with the slope = 16.3 $M^{-1}$.

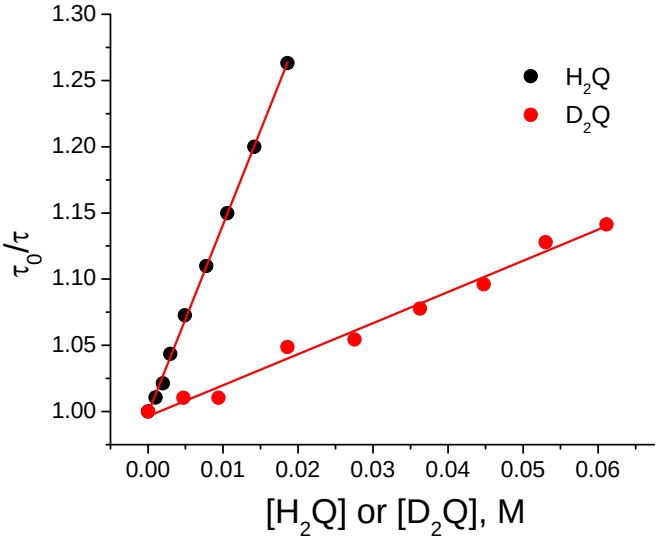


Figure S11. The bimolecular rate constant of reaction of $H_2Q$ and $D_2Q$ with *[**Ru**(**1**)]$^{2+}$ in $CH_3CN$. Kinetic isotope effect (KIE) was found to be $k_H/k_D = 6.2$.

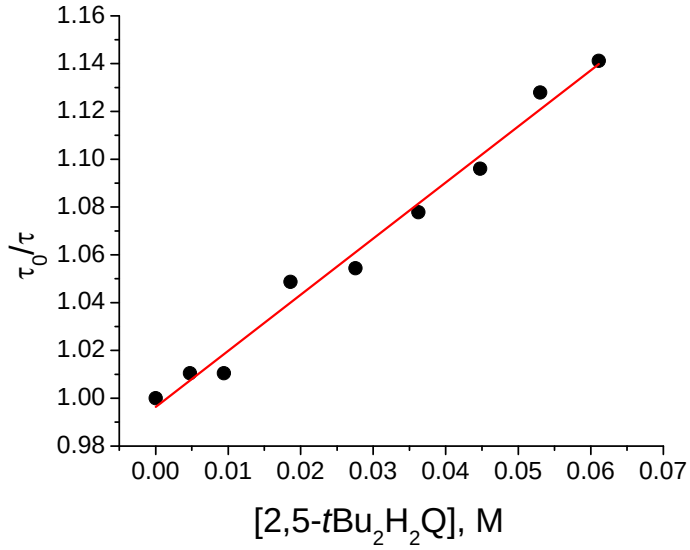


Figure S12. The bimolecular rate constant of reaction of $H_2Q(Bu^t)_2$ with *[**Ru**(**1**)]$^{2+}$ in $CH_3CN$.

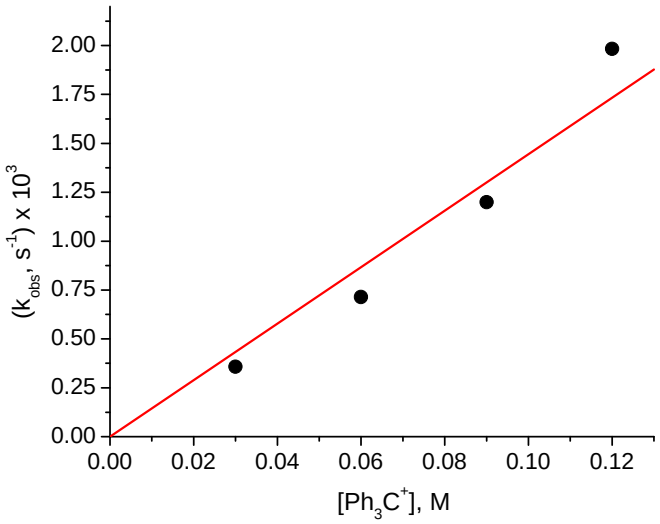


Figure S13. Observed rate of the formation of 626 nm band in the reaction between $[\mathbf{Ru}(\mathbf{1}HH)]^{2+}$ and the excess of triphenyl carbenium cation in acetonitrile plotted vs. concentration of $[Ph_3C]^+$. The rate constant obtained from the linear fit was $1.5 \times 10^{-2}$ $M^{-1}$ $s^{-1}$.

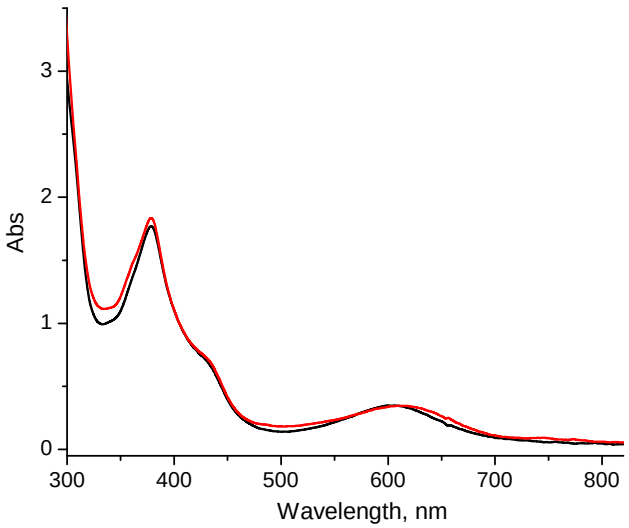


Figure S14. UV-vis spectra of the product of the reaction between $[Ru(\mathbf{1}HH)]^{2+}$ and $[Ph_3C]^+$ in methylene chloride (black); $[\mathbf{Ru}(\mathbf{1}H)]^{3+}$ in water pH = 1.

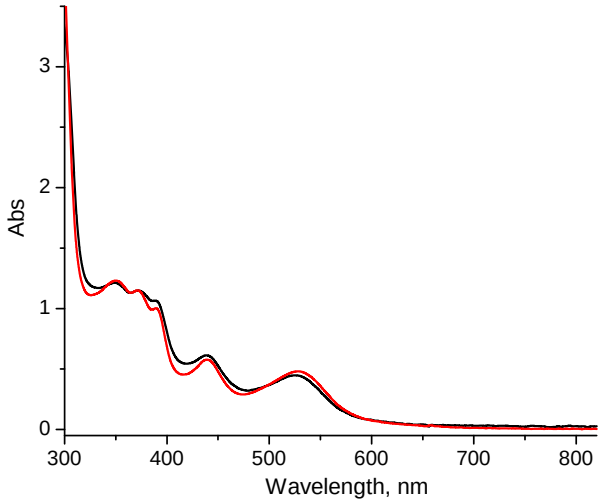


Figure S15. UV-vis spectra of the product of the reaction between [**Ru**(**1**HH)]$^{2+}$ and [$Ph_3C$]$^{+}$ in methylene chloride after addition of triethylamine (black); [**Ru**(**1**)]$^{2+}$ in water pH = 7.

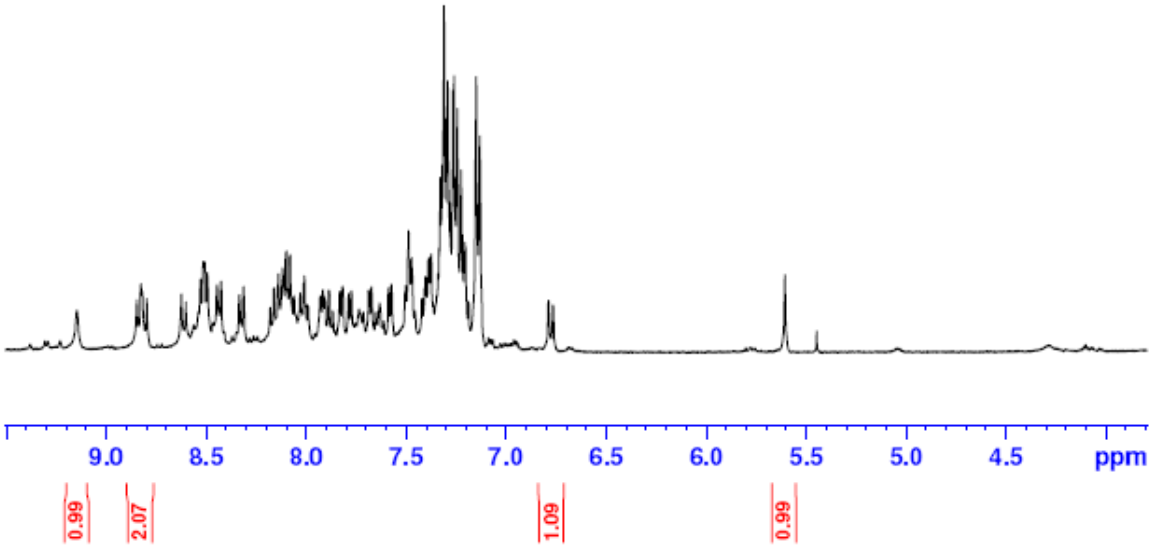


Figure S16. $^{1}$H NMR of reaction mixture of [**Ru**(**2**HH)]$^{2+}$ and [$Ph_3C$]$^{+}$ in $CD_3CN$, showing the formation of $Ph_3CH$ (5.6 ppm) in a 1:1 ratio with [**Ru**(**2**)]$^{2+}$. Characteristic peaks are integrated at 5.6 for $Ph_3CH$ and 9.07, 8.84-8.80, and 6.78 ppm for [**Ru**(**2**)]$^{2+}$.

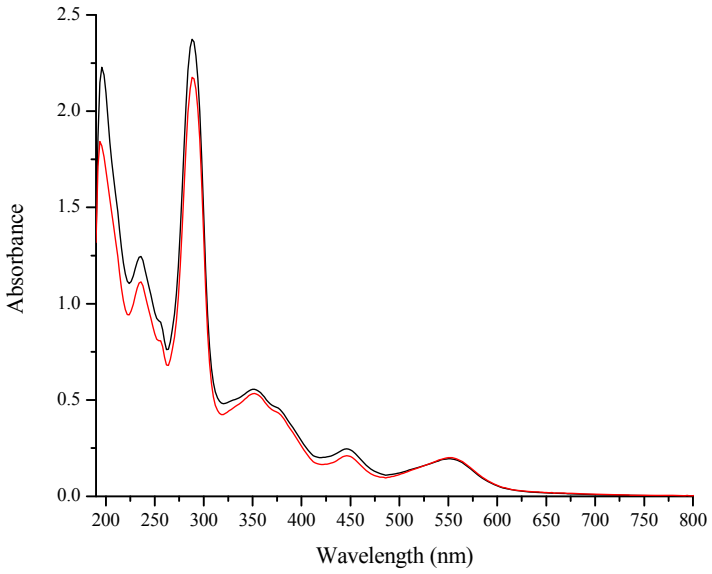


Figure S17. UV-vis spectra of [**Ru**(**2**)]$^{2+}$ before (red) and after (black) photochemical reduction, hydride donation, and purification in $CH_3CN$.

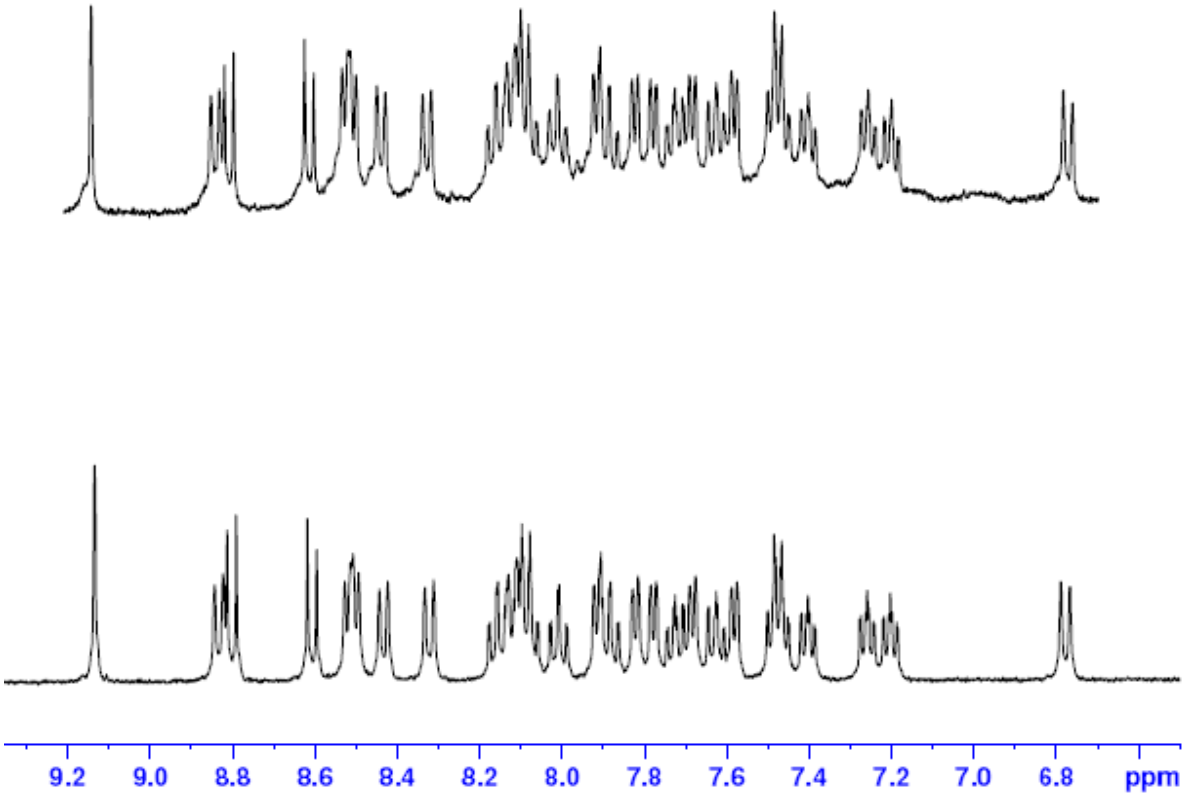


Figure S18. $^{1}$H NMR of [**Ru**(**2**)]$^{2+}$ starting material (bottom) and after photochemical reduction, hydride donation, and purification (top) in $CD_3CN$.

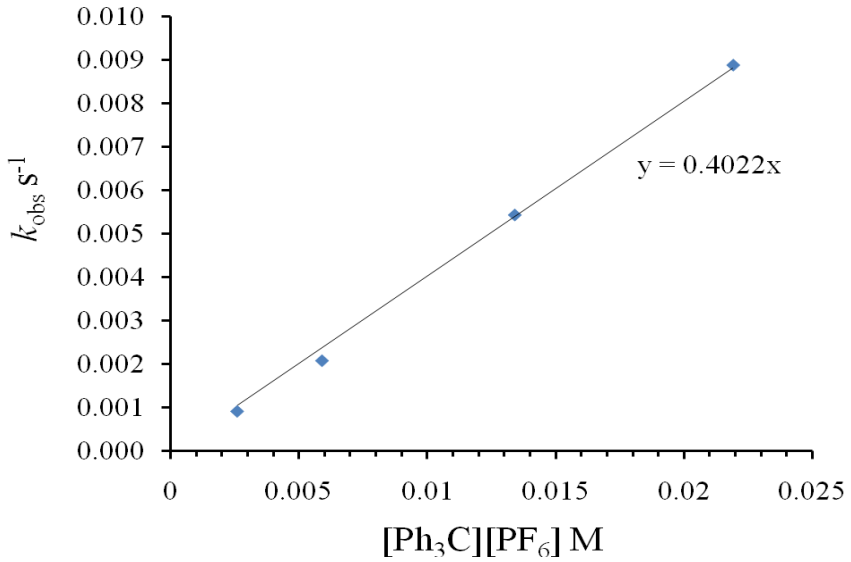


Figure S19. The bimolecular rate constant of hydride donation from [**Ru**(**2**HH)]$^{2+}$ to [Ph$_3$C]$^+$ in CH$_3$CN.

**Table S1.** Computed Geometrical Parameters of **Ru**(**2**) Species.

| | $[\mathbf{Ru}(\mathbf{2})]^{2+}$ | $[\mathbf{Ru}(\mathbf{2}^{\bullet-})]^{+}$ | $[\mathbf{Ru}(\mathbf{2}H^{\bullet})]^{2+}$ | $[\mathbf{Ru}(\mathbf{2}H)]^{3+}$ | $[\mathbf{Ru}(\mathbf{2}HH)]^{2+}$ |
|---|---|---|---|---|---|
| Ru–N pyridyl | 2.085 | 2.094 | 2.091 | 2.081 | 2.088 |
| Ru–N pbn | 2.157 | 2.141 | 2.166 | 2.159 | 2.171 |
| Ru–N $_{bpy1}$ (tr) | 2.101 | 2.091 | 2.122 | 2.126 | 2.118 |
| Ru–N $_{bpy1}$ | 2.095 | 2.083 | 2.096 | 2.101 | 2.095 |
| Ru–N $_{bpy2}$ (tr) | 2.089 | 2.092 | 2.090 | 2.085 | 2.088 |
| Ru–N $_{bpy2}$ | 2.092 | 2.081 | 2.091 | 2.096 | 2.090 |
| C9–H | 1.092 | 1.089 | 1.087 | 1.088 | 1.097, 1.102 |
| N10–H | n/a | n/a | 1.016 | 1.021 | 1.009 |
| C5–C12 | 1.407 | 1.424 | 1.430 | 1.398 | 1.513 |
| C12–C13 | 1.453 | 1.445 | 1.431 | 1.436 | 1.402 |
| C13–N10 | 1.369 | 1.382 | 1.404 | 1.370 | 1.409 |
| C9–C12 | 1.407 | 1.398 | 1.409 | 1.405 | 1.514 |
| C11–C12 | 1.453 | 1.467 | 1.449 | 1.427 | 1.420 |
| C11–N10 | 1.347 | 1.350 | 1.375 | 1.354 | 1.366 |
| N1–C11–C12–C9 | 179.97 | 179.99 | 179.44 | 179.69 | 176.82 |
| N $_{bpy}$···H | n/a | n/a | 2.069 | 2.036 | 2.083 |
| N10–N $_{bpy}$ | n/a | n/a | 3.047 | 3.035 | 3.066 |
| N10–H···N $_{bpy}$ | n/a | n/a | 163.9 | 165.5 | 163.9 |